Chapter 3

Event-Triggered Control of Power Electronics Converter

3.1 Introduction

In contemporary times, advanced control techniques play a crucial role in optimizing the operation of power electronic converters used in EVs. These techniques are essential for regulating the converter's output, enhancing dynamic performance, and effectively handling disturbances.

This chapter mainly explores the implementation of event-triggered control (ETC) in the linear parameter-varying (LPV) model of boost converters. This marks the commencement of a distinctive approach intended to enhance control strategies for these systems. This provides a unique viewpoint on improving control strategies for the systems. Boost converters, fundamental in power electronics, exhibit nonlinear dynamics that are explored within the LPV framework, setting the stage for a comprehensive investigation.

The focus of this research lies in the development and analysis of a duty-ratio-dependent controller designed for boost converters. This controller promises superior performance and demands less computational resources, aligning with the contemporary pursuit of efficiency and efficacy in control strategies. The stability of the proposed approach is systematically examined using the parameter-dependent

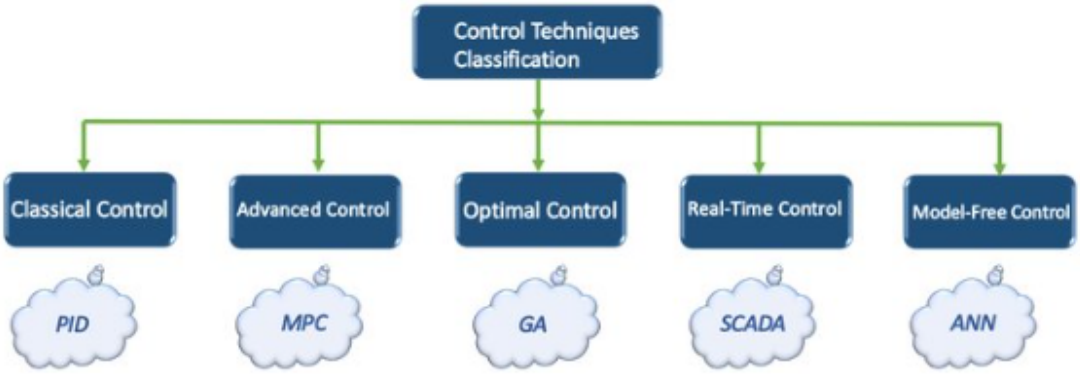

Figure 3.1: smart charging algorithm.

Lyapunov function (PDLF), providing a robust foundation for the subsequent discussions.

Furthermore, a crucial aspect addressed in this chapter is demonstrating that the inter-event time in the proposed ETC system is bound by a positive constant. This characteristic is pivotal in ensuring Zeno behavior-free performance, contributing to the reliability and predictability of the control system.

Drawing a comparison with earlier time-invariant synthesis techniques, the LPV formulation emerges as a promising avenue, offering heightened robustness and improved performance properties. The theoretical underpinnings laid out in this chapter set the stage for the exploration and validation of these ideas through both simulation and experimental results. Through this research, we aim to contribute to the advancement of control strategies for boost converters, with practical implications for diverse applications in power electronics and energy systems.

Since renewable energy has become more prevalent over the past few decades, and energy conversion technologies have been facing new challenges [114]. One of these difficulties is that several devices that store or create electrical energy (e.g., batteries [115], ultracapacitors [116], fuel cells [117], and solar panels [118] are constructed using low-voltage cells, which are frequently coupled in series to get a suitable voltage. The linking of a large number of cells in series increases the system's complexity and may degrade its performance due to cell variances (e.g., manufacturing discrep-

ancies) and varied operating circumstances (e.g., temperature). Furthermore, the output voltage of various sources of electrical energy varies significantly based on a variety of parameters, including the output current, state of charge, and solar radiation. In many applications, such as running electrical motors or injecting power into the grid a reasonably high and consistent voltage is frequently required. When this is the case, a step-up converter can be used to boost the source voltage to the level required by the application while maintaining a constant output voltage despite source voltage fluctuations [119].

3.2 Control in Power Electronics

Control in power electronic converters is essential to ensure proper operation, efficiency, and performance of these devices. Power electronic converters are widely used in various applications such as motor drives, renewable energy systems, electric vehicles, and more. The control strategies employed in these converters depend on the specific application and the type of converter used.

Here are some common control techniques and considerations: Voltage control, current control, pulse width modulation, Proportional-Integral (PI) Control, Voltage and Current Limiting, Feedback and Feedforward Control, Digital Signal Processing (DSP) Control, Sensorless Control are the some specific control strategy chosen depends on the application requirements, cost constraints, and the desired level of performance [120].

The two main categories of control techniques are conventional and advanced Fig. 3.1, given medium power applications. While conventional techniques such as PID (Proportional-Integral-Derivative) control and phase-locked loops (PLLs) are commonly utilized due to their simplicity and effectiveness, they may not deliver satisfactory results when faced with non-linear operating conditions or uncertain and variable system parameters.

This brings us to the domain of advanced control techniques specifically engineered to tackle these challenges and provide enhanced performance. Advanced control techniques encompass:

(i) Predictive control

(ii) Sliding mode control

(iii) H-infinity control

(iv) Adaptive control

these Control methods grounded in artificial intelligence [121].

The exploration of step-up converters, particularly boost converters, is of paramount significance in power electronics. When viewed through a control lens, these converters demonstrate nonlinear dynamics characterized by nonminimal phase behavior, as elucidated in [122]. To tackle this intricacy, this article transforms the nonlinear dynamics of a boost converter into a Linear Parameter-Varying (LPV) system, followed by the design of a controller dependent on duty ratio.

An LPV system essentially represents a linear system with multiple time-varying parameters, offering flexibility in simulating a diverse range of physical systems, as discussed in [123,124]. The tracking control for LPV modeling of boost converters is realized through an interpolation method, as exemplified in the investigation [125]. Additional noteworthy findings related to LPV systems are documented in [126,127].

This collective body of research contributes significantly to a deeper comprehension of the dynamics of boost converters and establishes a foundation for effective control strategies, particularly within the LPV framework.

3.3 Modelling and Event-Triggered Control of Power Electronics Converter

"Modeling and Event-Triggered Control of Power Converters" refers to the study and implementation of mathematical models and control strategies that utilize event-triggered approaches in the operation of power converters. This field involves developing accurate mathematical representations (models) of power converters and employing event-triggered control techniques to optimize their performance.

- **Modeling of Power Converters**: The modeling aspect involves creating mathematical representations that describe the behavior and dynamics of power con-

verters. This includes understanding the relationships between input and output variables, the effects of different components, and the overall system response.

- **Event-Triggered Control**: ETC is a control strategy where the updates of the control signal are triggered by specific events rather than occurring at regular intervals. These events could be changes in the system state, deviations from desired values, or other predefined conditions.

- **Applications and Importance**:
  (i) The application of modeling and event-triggered control in power converters is crucial for enhancing efficiency, reducing computational demands, and optimizing resource utilization. By developing accurate models, researchers and engineers can better understand the behavior of power converters under different conditions.
  (ii) Event-triggered control strategies offer advantages in reducing the frequency of control updates, which can lead to energy savings and improved overall system performance. This is particularly relevant in applications where resources, bandwidth, and computational power are limited [128].

  The above-mentioned outcomes utilized a continuous deployment approach for LPV systems and boost converters. Nevertheless, practical systems necessitate reduced resource usage, bandwidth, and computational demands. Numerous studies have explored the advantages of employing Event-Triggered Control (ETC) in these situations [129]. The identical event-triggered methodology is investigated for nonlinear multiagent systems in [130]. Other notable studies focusing on event-triggered strategies for estimation issues in Markov jump systems can be found in [131, 132]. Due to the advantages of this approach, numerous researchers have applied it to address the challenge of voltage regulation in power converters. In [133], an event-triggered PI controller for voltage regulation in a DC-DC buck converter is scrutinized. Recently, a presented event-triggered approach addresses microrobot position control. This similar approach addresses the missile guidance problem in [134]. Utilizing the findings discussed earlier regarding boost converters and LPV systems, we integrated the advantages of Event-Triggered Control (ETC) to formulate an ETC for the LPV framework of a boost converter. To the author's knowledge, this marks the inaugural endeavor to devise an ETC tailored specifically for the LPV modeling

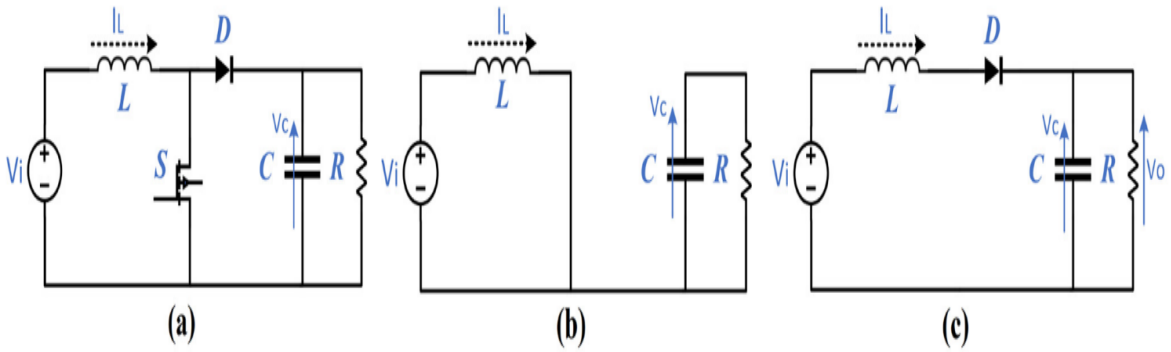

Figure 3.2: Boost converter circuit diagram and switching loss: (a) Circuit schematic; (b) Switch is on; (c) Switch is off.

of boost converters. The contribution of this brief is outlined as follows:

(1) Introducing LPV modeling of boost converters, offering a less conservative approach compared to time-invariant synthesis.

(2) introducing a synthesis approach dependent on parameters to create controllers tailored to specific parameters. This chapter provides details on system modeling and problem formulation, the essential outcomes with simulation and experimental results .

Notation: For a function $f(x)$, its upper right Dini derivative is defined by $\mathcal{D}^+ f(x) = \lim_{\tau \to 0^+} \sup\left((f(x+\tau) - f(x))/\tau\right)$

3.4 Problem Formulation and Objective Determination

Fig. 3.2(a) shows a boost converter circuit diagram. In this chapter, the inductor current is represented by I_L, while the capacitor voltage is represented by V_c. Let $x = \begin{bmatrix} I_L & V_c \end{bmatrix}^T$ is the state variable, $u = V_i$ is the input variable, and $y = \begin{bmatrix} I_L & V_o \end{bmatrix}^T$ is the output variable. When the switch is on and off, the boost converter has two operation states, as shown in Fig. 3.2(b) and (c).

If the switch (S) is on, as seen in Fig. 3.2(b), the state-space can be defined as

follows:

$$\dot{x} = \begin{bmatrix} 0 & 0 \\ 0 & -\frac{1}{CR} \end{bmatrix} x + \begin{bmatrix} \frac{1}{L} \\ 0 \end{bmatrix} u \triangleq A_1 x + B_1 u$$
$$y = \begin{bmatrix} 1 & 0 \\ 0 & 1 \end{bmatrix} x \triangleq C_1 x \tag{3.1}$$

When the switch (S) is turned off, as seen in Fig. 3.2(c), the state-space form can be written as follows:

$$\dot{x} = \begin{bmatrix} 0 & -\frac{1}{L} \\ \frac{1}{C} & -\frac{1}{CR} \end{bmatrix} x + \begin{bmatrix} \frac{1}{L} \\ 0 \end{bmatrix} u \triangleq A_2 x + B_2 u$$
$$y = \begin{bmatrix} 1 & 0 \\ 0 & 1 \end{bmatrix} x \triangleq C_2 x \tag{3.2}$$

Consider the boost converter's duty ratio is $D = T_{on}/T$, where T is the switching period of the switch and T_{on} is the time interval in which the switch is on in the switching period. Let $D_1 = D$ and complementary duty ratio $D_2 = 1 - D$. The boost converter's averaged state-space representation [125] can be determined as follows:

$$A(D) \triangleq D_1 A_1 + D_2 A_2, \quad B(D) \triangleq D_1 B_1 + D_2 B_2$$
$$C(D) \triangleq D_1 C_1 + D_2 C_2$$

$$\begin{cases} \dot{x} &= A(D)x + B(D)u \\ y &= C(D)x \end{cases} \tag{3.3}$$

Remark 1: The state-space averaging technique assesses the system's performance over a considerably longer time span than its switching period. It involves determining the average system state by assigning weights to each state-space element based on its time duration within one complete period.

Analyzing the system outlined in (3.3), it is apparent that the state-space of the boost converter undergoes substantial changes when the duty ratio $D \in (0, 1)$ is modified. Moreover, the equation (3.3) includes the product of D and the state

variables x. This introduces nonlinearity in the responses of state spaces to variations in the duty ratio D. The ETC presented for consideration is detailed as follows:

$$u = K\left(D(t_k)\right) x(t_k), \quad \forall t \in [t_k, t_{k+1}) \tag{3.4}$$

where $K\left(D(t_k)\right) \in \mathbb{R}^{1\times 2}$ is the parameter varying gain matrix to be designed. By substituting the proposed control (3.4) into the system (3.3), the closed-loop system becomes

$$\dot{x} = A(D)x + B(D)K(D(t_k))x(t_k) \tag{3.5}$$

Consider defining the time sequence for event-triggered sampling denoted as t_k, involving variables x and D for $k \in \mathbb{N}$. Subsequently, the measurement errors for the time interval $t \in [t_k, t_{k+1})$ can be articulated as follows:

$$e_x \triangleq x(t_k) - x, \quad e_D \triangleq D(t_k) - D. \tag{3.6}$$

According to (3.6), (3.5) can be expressed as

$$\dot{x} = A(D)x + B(D)K\left(e_D + D\right)\left(e_x + x\right) \tag{3.7}$$

To avoid the notational complexity, we are not writing explicit function .
For the system (3.7), the function $V(x, D)$ is called the parameter-dependent input to state exponentially stable Lyapunov function if there exists positive constant $\lambda, \underline{\mu}, \bar{\mu}, \mu$ with $\underline{\mu} \leq \bar{\mu}$ and a function γ which satisfy

$$\begin{aligned}
&\frac{\partial V}{\partial x}\left(A(D)x + B(D)K\left(e_D + D\right)\left(e_x + x\right)\right) + \lambda V(x, D) \\
&\qquad \leq -\mu\|x\|^2 + \gamma(\|e_D\|)\|e_x\|\|x\| \\
&\underline{\mu}\|x\|^2 \leq V(x, D) \leq \bar{\mu}\|x\|^2
\end{aligned}$$

3.5 Main Results

The key findings of the chapter are outlined in this section. The subsequent part provides an account of the event-triggering scheme presented within the context of this thesis chapter.

$$\|e_x\| \geq \frac{\alpha - 2\bar{\rho}\bar{\beta}\sum_{i=1}^{2}\left\{\bar{k}_{ai}\|e_{Di}\|\right\}}{2\bar{\rho}\bar{\beta}\bar{k} + 2\bar{\rho}\bar{\beta}\sum_{i=1}^{2}\left\{\bar{k}_{ai}\|e_{Di}\|\right\}}\|x\| \tag{3.8}$$

where $e_{D_i} = D_i(t_k) - D_i$ for $i = 1, 2$, and $\sum_{i=1}^{2} D_i = 1$

When the condition (3.8) is satisfied, the control undergoes an update to fulfill the specified stability requirement.

$$\|e_x\| \leq \frac{\alpha - 2\bar{\rho}\bar{\beta}\sum_{i=1}^{2}\left\{\bar{k}_{ai}\|e_{Di}\|\right\}}{2\bar{\rho}\bar{\beta}\bar{k} + 2\bar{\rho}\bar{\beta}\sum_{i=1}^{2}\left\{\bar{k}_{ai}\|e_{Di}\|\right\}}\|x\|. \tag{3.9}$$

The previously discussed fact is illustrated in the following theorem.

Theorem 1: Consider the closed-loop system (3.7). For a given positive scalars α, λ and matrix $K(D)$) if there exists a positive definite matrix $P(D)$, such that the following inequality holds

$$\begin{aligned} &A^T(D)P(D) + P(D)A(D) + K^T(D)B^T(D)P(D) \\ &\quad + P(D)B(D)K(D) + \dot{P}(D) + \lambda P(D) + \alpha I < 0 \end{aligned} \tag{3.10}$$

where, $\max_D \{\|P(D)\|\} \leq \bar{\rho}$,

$$\begin{aligned} &\max_D \{\|B(D)\|\} \leq \bar{\beta}, \qquad \max_D \{\|K(D)\|\} \leq \bar{k} \\ &\max_D \left\{ \left\| \int_0^1 \frac{\partial K(z)}{\partial z_i}|_{z_i = D_i + \tau e_{Di}} d\tau \right\| \right\} \leq \bar{k}_{ai}, \quad i = 1, 2 \end{aligned}$$

Then, the system (3.7) is said to be exponentially stable.

Proof. Consider the parameter dependent Lyapunov function as $V(x, D) = x^T P(D)x$. Using upper right Dini derivative, differentiating $V(x, D)$ along solutions x of the system (3.7) yields

$$\begin{aligned} &\dot{V}(x, D) + \lambda V(x, D) \\ &= \dot{x}^T P(D)x + x^T P(D)\dot{x} + x^T \dot{P}(D)x + \lambda x^T P(D)x \\ &= 2\left[x^T P(D)\left\{A(D)x + B(D)\left(K(D + e_D)\right)(x + e_x)\right\}\right] \\ &\quad + x^T \dot{P}(D) + \lambda x^T P(D)x \end{aligned} \tag{3.11}$$

where $K(D+e_D) = K(D) + \sum_{i=1}^{2}\left\{e_{Di}\bar{K}_i(D, e_D)\right\}$, $\bar{K}_i(D, e_D) = \int_0^1 \frac{\partial K(z)}{\partial z_i}|_{z_i = D_i + \tau e_{Di}} d\tau$, $\tau =$

$(0, 1)$. Accordingly, we have

$$\begin{aligned}
&\dot{V}(x, D) + \lambda V(x, D) \qquad (3.12)\\
&= x^T \left[A^T(D)P(D) + P(D)A(D) + K^T(D)B^T(D)P(D)\right.\\
&\quad \left. + P(D)B(D)K(D) + \dot{P}(D) + \lambda P(D)\right] x\\
&\quad + 2x^T P(D)B(D)K(D)e_x + 2x^T P(D)B(D)\times\\
&\quad \left[\sum_{i=1}^{2} \left\{e_{Di}\bar{K}_i(D, e_D)\right\} + \sum_{i=1}^{2} \left\{e_{Di}\bar{K}_i(D, e_D)\right\}\right] \qquad (3.13)\\
&\leq -\alpha x^T x + 2x^T P(D)B(D)K(D)e_x + 2x^T P(D)B(D)\\
&\quad \times \left[\sum_{i=1}^{2} \left\{e_{Di}\bar{K}_i\right\} x + \sum_{i=1}^{2} \left\{e_{Di}\bar{K}_i\right\} e_x\right] \qquad (3.14)
\end{aligned}$$

Earlier defined norm bounds of the known matrices are applied to the inequality (3.14), which provides

$$\begin{aligned}
\dot{V}(x, D) + \lambda V(x, D) \leq -\|x\| \Bigg[&\alpha\|x\| - 2\bar{\rho}\bar{\beta}\bar{k}\|e_x\|\\
&- 2\bar{\rho}\bar{\beta}\sum_{i=1}^{2} \left(\left\{\bar{k}_{ai}\left\|e_{Di}\right\|\right\}\|x\| + \left\{\bar{k}_{ai}\left\|e_{Di}\right\|\right\}\|e_x\|\right)\Bigg] \qquad (3.15)
\end{aligned}$$

From the inequality (3.15) and stability condition (3.9), we can show that

$$\dot{V}(x, D) + \lambda V(x, D) < 0 \qquad (3.16)$$

Accordingly, one can obtain $V \leq V(t_k)e^{-\lambda(t-t_k)}, \forall t \in [t_k, t_{k+1})$ Thus, the system (3.7) is exponentially stable.

3.5.1 Analysis of the Inter-event Time

This section presents an examination devoid of Zeno phenomena, with the following theorem explaining this observation. Zeno behavior refers to a phenomenon in control systems where an infinite number of events or control updates occur in a finite amount of time. This is an undesirable situation because it implies that the system would require an infinitely fast update rate, which is not feasible in real-world applications due to physical limitations in computational and communication resources. In the context of event-triggered control, Zeno behavior can cause the system to become unstable or unmanageable.

Theorem 2: Consider the closed-loop system (3.7). For any initial value of $x(t_0)$, if there exist positive constants η and $\bar{h}_i > 0$ that satisfy $\sum_{i=1}^{2} \left\{ \bar{k}_{ai} \| e_{Di} \| \right\} \leq \eta$ and $\| \dot{D} \| \leq \bar{h}_i$ for $i = 1, 2$. Then, the inter-event time $T_k = t_{k+1} - t_k$ is obtained by the event-triggered scheme (3.8) is lower bounded by the constant

$$\tau = \min \left\{ \frac{\eta}{\sum_{i=1}^{2} \left\{ \bar{k}_{ai} \ \bar{h}_i \right\}}, T_k \right\} \tag{3.17}$$

with

$$T_k = \frac{\bar{\alpha}}{\bar{\beta}^2 \bar{k}^2} \left[\ln \left(1 + \frac{\bar{\alpha}}{\bar{\beta}\bar{k}} \right) - \ln \left(1 + \frac{\bar{\alpha}}{\bar{\beta}\bar{k}} \frac{1}{1 + \frac{\alpha - 2\bar{\rho}\bar{\beta}\eta}{2\bar{\rho}\bar{\beta}\bar{k} + 2\bar{\rho}\bar{\beta}\eta}} \right) \right] \tag{3.18}$$

$$\begin{aligned}
&\max_{d \in \mathcal{Q}} \{ \| A(D) \| \} \leq \bar{\alpha}, \qquad \max_{d \in \mathcal{Q}} \{ \| P(D) \| \} \leq \bar{\rho}, \\
&\max_{d \in \mathcal{Q}} \{ \| B(D) \| \} \leq \bar{\beta}, \qquad \max_{d \in \mathcal{Q}} \{ \| K(D) \| \} \leq \bar{k}, \\
&\max_{d \in \mathcal{Q}} \left\{ \left\| \int_0^1 \frac{\partial K(z)}{\partial z_i} |_{z_i = d_i + \tau e_{di}} d\tau \right\| \right\} \leq \bar{k}_{ai}, \quad i = 1, 2.
\end{aligned}$$

Proof. From the closed-loop system (3.7), we have

$$\begin{aligned}
\| \dot{x} \| &\leq \| A(D) + B(D) K(D + e_D) \| \, \| x \| + \| B(D) K(D + e_D) \| \\
&\quad \times \| e_x \| \leq \left(\bar{\alpha} + \bar{\beta}\bar{k} \right) \| x \| + \bar{\beta}\bar{k} \| e_x \|
\end{aligned} \tag{3.19}$$

One can show that

$$\begin{aligned}
\mathcal{D}^+ \left(\frac{\| e_x \|}{\| x \|} \right) &= \mathcal{D}^+ \frac{\left(e_x^T e_x \right)^{1/2}}{\left(x^T x \right)^{1/2}} \\
&= \frac{\left(e_x^T e_x \right)^{-1/2} e_x^T \dot{e}_x \left(x^T x \right)^{1/2} - \left(x^T x \right)^{-1/2} x^T \dot{x} \left(e_x^T e_x \right)^{1/2}}{x^T x} \\
&\leq \frac{\| e_x \| \, \| \dot{x} \|}{\| e_x \| \, \| x \|} + \frac{\| x \| \, \| \dot{x} \| \, \| e_x \|}{\| x \| \, \| x \| \, \| x \|} = \left(1 + \frac{\| e_x \|}{\| x \|} \right) \frac{\| \dot{x} \|}{\| x \|} \\
&\leq \left(1 + \frac{\| e_x \|}{\| x \|} \right) \left(\bar{\alpha} + \bar{\beta}\bar{k} + \bar{\beta}\bar{k} \frac{\| e_x \|}{\| x \|} \right) \\
&= \bar{\alpha} + \bar{\beta}\bar{k} + \left(\bar{\alpha} + 2\bar{\beta}\bar{k} \right) \frac{\| e_x \|}{\| x \|} + \bar{\beta}\bar{k} \left(\frac{\| e_x \|}{\| x \|} \right)^2
\end{aligned} \tag{3.20}$$

Consider $\xi = \frac{\| e_x \|}{\| x \|}$ and $e_x = 0$ yields $\xi = 0$. Then, we have the estimation $\mathcal{D}^+ \xi \leq \bar{\alpha} + \bar{\beta}\bar{k} + \left(\bar{\alpha} + 2\bar{\beta}\bar{k} \right) \xi + \bar{\beta}\bar{k}\xi^2$. Suppose

$$\dot{\phi} \leq \bar{\alpha} + \bar{\beta}\bar{k} + \left(\bar{\alpha} + 2\bar{\beta}\bar{k} \right) \phi + \bar{\beta}\bar{k}\phi^2 \tag{3.21}$$

with $\phi_0 = 0$. We reach at $\xi \leq \phi(t, \phi_0)$ by the comparison principle [129].

Lets assume the previous triggering instant is t_k. When $\frac{\|e_x\|}{\|x\|}$ evolves from 0 to $\Gamma_m(\|e_D\|)$, the next trigger will occur under the condition (3.8). According to the comparison principle, the inter-event time $T_k = t_{k+1} - t_k$ is lower bound by the time that ϕ evolves from 0 to $\Gamma_m(\|e_D\|)$. After solving the differential equation (3.21), we obtain that

$$T_k = \frac{\bar{\alpha}}{\bar{\beta}^2\bar{k}^2}\left[\ln\left(1+\frac{\bar{\alpha}}{\bar{\beta}\bar{k}}\right) - \ln\left(1+\frac{\bar{\alpha}}{\bar{\beta}\bar{k}}\frac{1}{1+\Gamma_m(\|e_D\|)}\right)\right] \tag{3.22}$$

When $t = t_k$, the equality $\|e_{Di}\| = 0$ holds, which yields $\Gamma(\|e_D\|) = \Gamma_{\max} = \frac{\alpha}{2\bar{\rho}\bar{\beta}\bar{k}} > 0$. There is no trigger at $t = t_k$ because the triggering interval

$$T_k = \frac{\bar{\alpha}}{\bar{\beta}^2\bar{k}^2}\left[\ln\left(1+\frac{\bar{\alpha}}{\bar{\beta}\bar{k}}\right) - \ln\left(1+\frac{\bar{\alpha}}{\bar{\beta}\bar{k}}\frac{1}{1+\frac{\alpha}{2\bar{\rho}\bar{\beta}\bar{k}}}\right)\right] > 0 \tag{3.23}$$

must be satisifed. Therefore, there exists a positive constant η satisfying $\sum_{i=1}^{2}\left\{\bar{k}_{ai}\|e_{Di}\|\right\} \leq \delta$, we get $\Gamma(\|e_D\|) \geq \left(\frac{\alpha - 2\bar{\rho}\bar{\beta}\bar{k}_a\eta}{2\bar{\rho}\bar{\beta}\bar{k}+2\bar{\rho}\bar{\beta}\bar{k}_a\eta}\right) \triangleq \varpi$. Since, the next trigger only occurs when $\|e_x\| = \Gamma(\|e_D\|)\|x\|$, we deduce that the next trigger can not happen before the time of $\frac{\|e_x\|}{\|x\|} = \varpi$. The equality $\sum_{i=1}^{2}\left\{\bar{k}_{ai}\|e_{Di}\|\right\} = \eta$ holds when it is at the time t. Using differential mean value theorem [126] one can show that

$$\begin{aligned}\eta = \sum_{i=1}^{2}\left\{\bar{k}_{ai}\|e_{Di}\|\right\} = \sum_{i=1}^{2}\left\{\bar{k}_{ai}\|D_i - D_i(t_k)\|\right\} = \\ \sum_{i=1}^{2}\left\{\bar{k}_{ai}\|\dot{D}(\varpi_i)\|\right\}(t-t_k) \leq \sum_{i=1}^{2}\left\{\bar{k}_{ai}\ \bar{h}_i\right\}(t-t_k)\end{aligned} \tag{3.24}$$

where $\varpi_i \in (t_k, t)$. Hence, we get $t - t_k \geq \frac{\eta}{\sum_{i=1}^{2}\left\{\bar{k}_{ai}\ \bar{h}_i\right\}} > 0$. Employing (3.22) we can show that $T_k > 0$

Based on (3.17) and $T_k > 0$, we can demonstrate that the inter-event time is lower bound by the positive constant.

Remark 2: Considering the utmost upper bounds for the parameter-dependent matrices in Theorems 1 and 2, it is essential to acknowledge that this choice may lead to conservative outcomes.

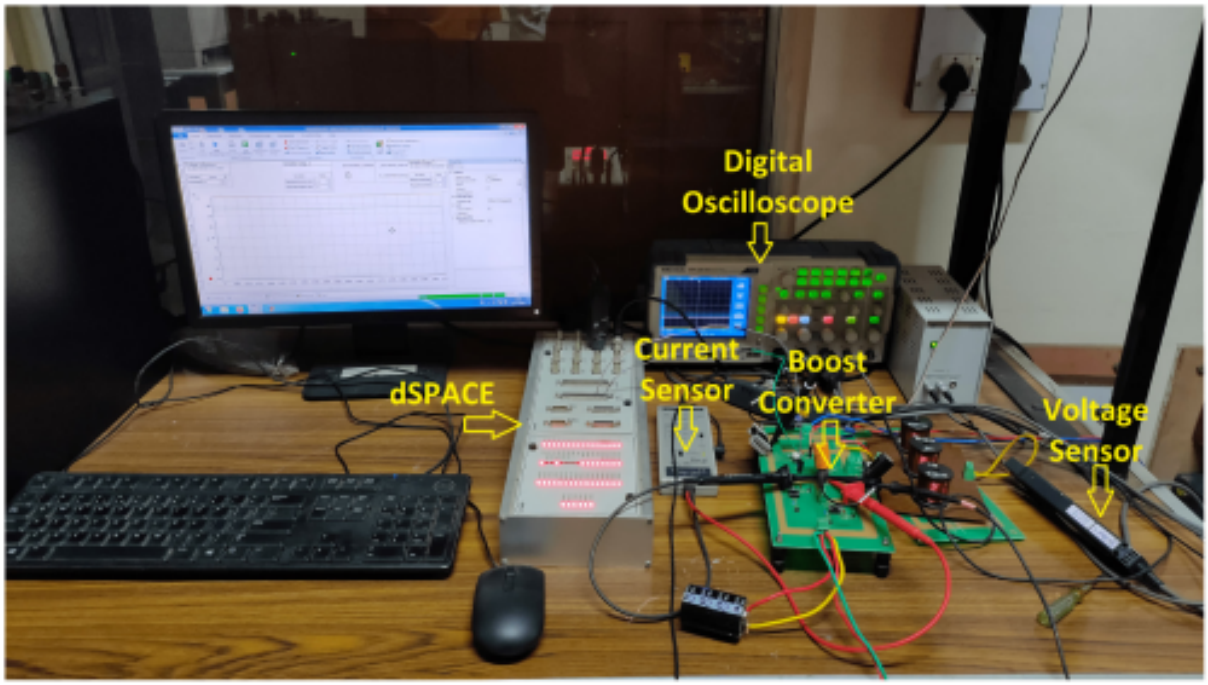

Figure 3.3: Hardware setup of the boost converter.

3.6 Numerical Simulation and Experimental Results

A boost converter designed with the following specifications: $V_i = 24\text{V}$, $V_{\text{ref}} = 48\text{V}$, $I_{\text{ref}} = 2\text{A}$, $R = 20\Omega$, $L = 1120\mu\text{H}$, and $C = 100\mu\text{F}$ is use for both the simulation and experimental tests. Control and data acquisition are managed through the MATLAB/SIMULINK interface with the dSPACE MicroLabBox. Fig. 3.3 illustrates the hardware configuration. We evaluate the controller's performance in two situations:

(1) Regulating output voltage under varying input voltage.

(2) Maintaining output voltage regulation with a changing load.

The control input is chosen as $u = u(t_k) = K(D(t_k))x(t_k)$. The design parameters are $K(D) = \begin{bmatrix}0.01 & 0.3\end{bmatrix} + D\begin{bmatrix}0.025 & 0.9\end{bmatrix}$, $D \in (0, 1)$ and scalers are $\alpha = 5, \lambda = 0.7$. They were all chosen to give satisfactory responses.

To illustrate the effectiveness of the suggested methodology, we compared our findings with those of a related study [133]. An event-triggered PI controller was designed for the DC-DC converters in [133]. The controller's specifications are as follows: $u = K_i \int_0^t (V_{\text{ref}} - V_o(t_k))dt + K_p(V_{\text{ref}} - V_o(t_k))$, where $K_p = 0.0175$ and

$K_i = 0.5$ are the controller gains.

3.6.1 Simulation Results

(i) Regulation of output voltage when input voltage changes

Variable input voltages are applied to the boost converter while maintaining the reference output voltage at 48V. Initiating with an input voltage of 21V and incrementing it to 29V, Fig. 3.4(a) depicts the output voltage response. The simulation results affirm that the proposed method significantly reduces the settling time by 60-70 % while ensuring the desired voltage regulation. Additionally, the proposed approach promptly restores the output voltage to the required level with the change in input voltage at $t = 0.5s$. In Fig. 3.4(b), the graph illustrates the response of the inductor current. The evolution of the control signal, where the duty ratio exhibits a zig-zag pattern due to the implementation of ETCs, is presented in Fig. 3.4(c). Events related to the triggering condition are indicated in Fig. 3.4(d) and (e), where an event flag is set to 1 upon satisfying the triggering condition.

(ii) Regulating Output Voltage under Load Variations

The boost converter experiences varying load currents, with adjustments made to ensure the output voltage remains at 48V. The initial load current of 2A is gradually increased to 4A. The graph illustrates the voltage response in Fig. 3.5(a). As observed in the previous scenario, the proposed method substantially reduces settling time by approximately 60-70 %. This efficiency is also evident in effectively handling load changes at $t = 0.5s$. Fig. 3.5(b) showcases the response of the inductor current. Furthermore, Fig. 3.5(c) visually tracks the evolution of duty ratios with varying load currents. The occurrence of events related to the triggering condition is depicted in Fig. 3.5(d) and (e), where an event flag is set to 1 upon satisfying the triggering condition.

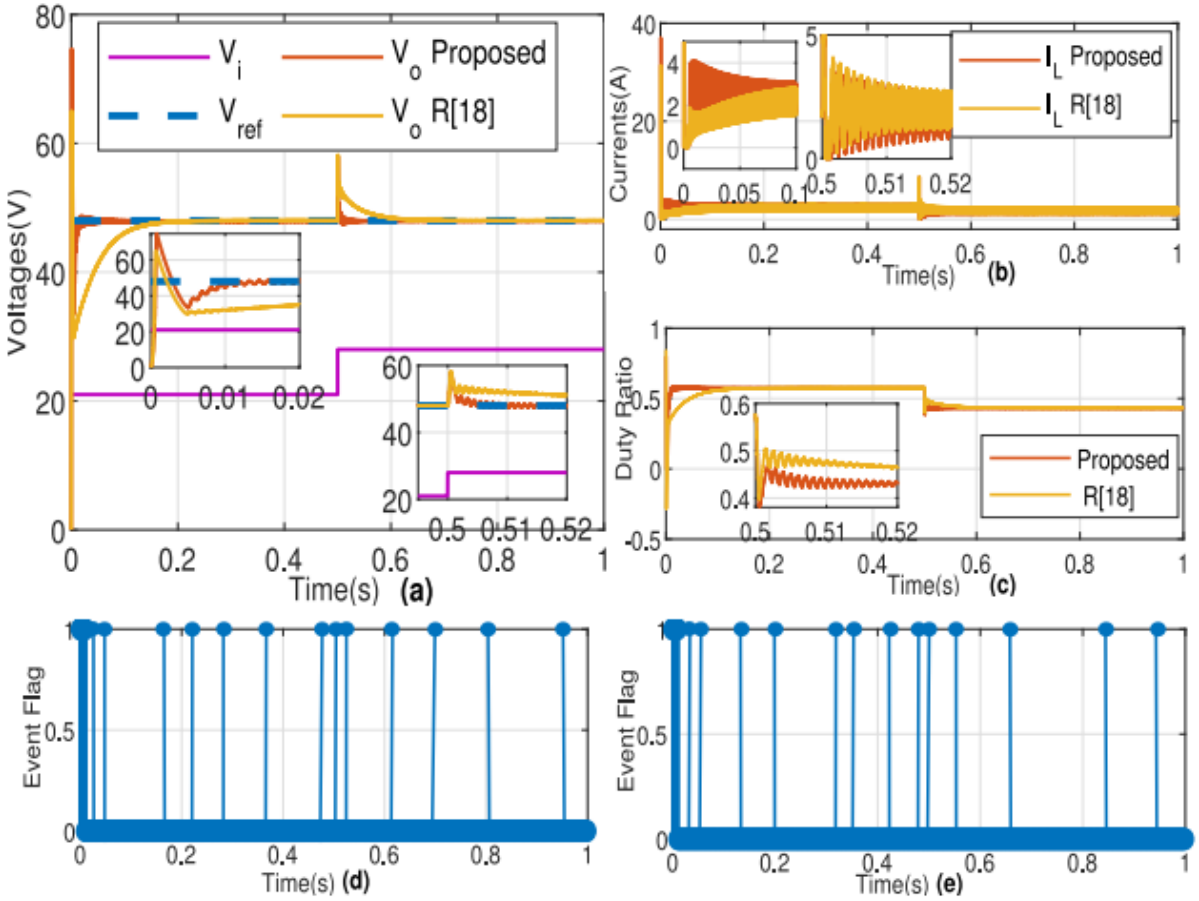

Figure 3.4: Simulation response with varying input voltage (21V to 29V): (a) Voltages; (b) Currents; (c) Duty ratio; (d) Proposed event flag; (e) R[18] event flag.

3.6.2 Experimental Results

The experimental results for the boost converter, implementing the proposed approach, are demonstrated in Fig. 3.6(a) and (b).

In Fig. 3.6(a), the variation in input voltage from 21V to 29V at $t = 0.5s$, with a constant load of $R = 48\Omega$, results in the output voltage remaining around 48V. Similarly, in Fig. 3.6(b), when the load transitions from 48Ω to 24Ω at $t = 0.5s$, with a constant input voltage of $V_i = 21V$, the output voltage maintains its proximity to 48V. Consequently, alterations in input voltage and load have minimal impact on the output voltage regulation.

In Fig. 3.6 (a), the top waveform (cyan color) indicates the input voltage V_{in}, the middle waveform (purple color) depicts the output voltage V_{out} and the lower wave-

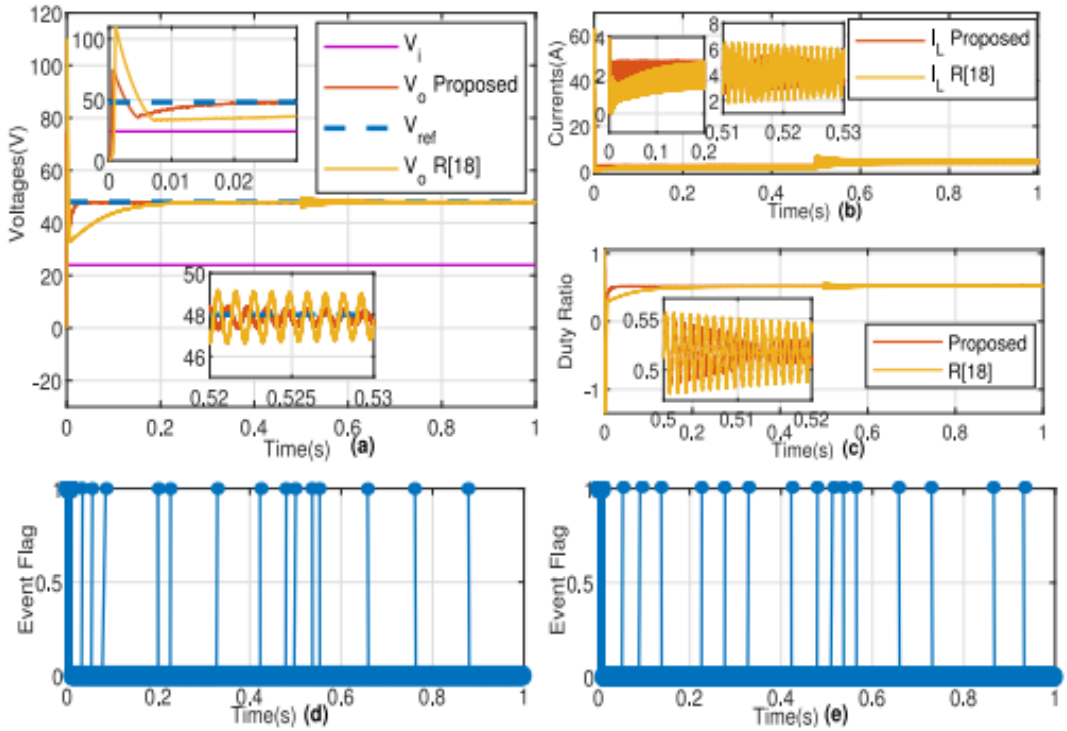

Figure 3.5: Simulation response with varying load (48Ω to 24Ω): (a) Voltages; (b) Currents; (c) Duty ratio; (d) Proposed event flag; (e) R[18] event flag.

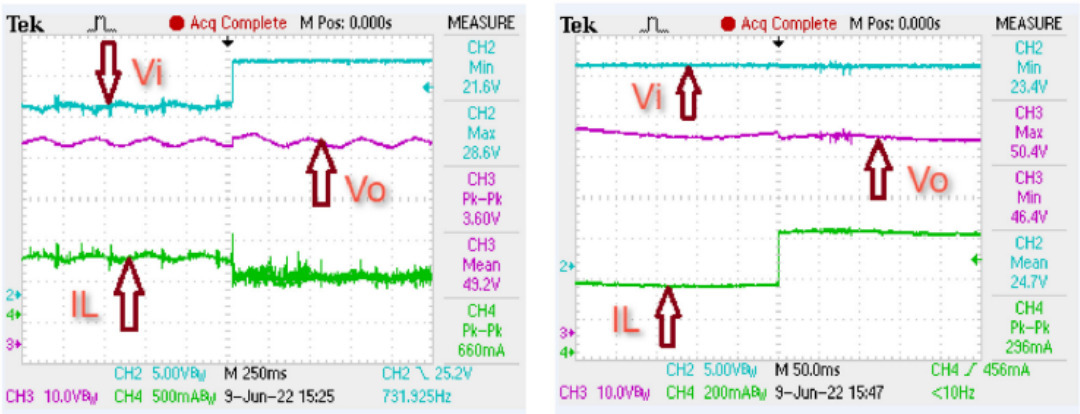

Figure 3.6: (a) Experimental response with varying input voltage (21V to 29V); (b) Experimental response with varying load resistor (48Ω to 24Ω).

form (green color) shows the inductor current I_L. Similarly, in Fig. 3.6 (b), the top waveform (cian color) indicates the input voltage V_{in}, the middle waveform (purple color) depicts the output voltage V_{out} and the lower waveform (green color) shows the inductor current I_L. In the experimental results depicted in Fig. 3.6(a) and (b), oscillations are noticeable in the output voltage of the converter due to the event-triggered characteristics of the control signal.

Impact of the converter's performance in EV-related applications: The selected boost converter configuration is particularly significant for EV on-board chargers, renewable energy integration, and energy storage systems. In these applications, maintaining stable voltage regulation despite variations in input voltage and load conditions is crucial for efficient power conversion. For instance, in EV on-board chargers, fluctuations in grid or solar PV input voltage necessitate robust regulation to ensure reliable battery charging. Similarly, in vehicle-to-vehicle (V2V) charging scenarios, where one EV supplies power to another, stable voltage control is essential to optimize power transfer and protect battery health.

The selection of control inputs and evaluation scenarios in this study were specifically designed to replicate these real-world operating conditions. By analyzing the controller's performance under varying input voltage and dynamic load changes, we aimed to ensure its effectiveness in practical applications.

Experimental findings in establishing system reliability: The reliability of the system is validated through experimental tests under varying input voltage conditions and dynamic load changes. The controller consistently maintains output voltage regulation despite these disturbances, ensuring stable and predictable performance. The event-triggered control approach enhances reliability by reducing unnecessary control updates while effectively responding to system variations.Moreover, the proposed method minimizes transient deviations and ensures steady-state accuracy, further reinforcing its reliability in practical applications. The introduction of a lower bound on the inter-event time prevents excessive switching (Zeno behavior), ensuring sustained stability and long-term operational reliability.

Scalability for Large-Scale Systems : While the chapter 4 primarily focuses on validating the proposed controller for a laboratory-scale boost converter, the scalability of the control strategy for large-scale systems can be inferred as follows:

• The LPV modeling framework allows for extending the control approach to higher-power converters with dynamically changing operating conditions.

• The event-triggered mechanism reduces the computational burden, making the approach suitable for embedded systems in large-scale applications, such as electric vehicle charging infrastructure and grid-integrated renewable energy systems.

• The stability analysis provided in the paper guarantees Zeno behavior-free operation, ensuring practical feasibility even when applied to large-scale multi-converter systems.

3.7 Summary

Based on the simulation and experimental findings, the presented technique offers enhanced steady-state and transient performance. Consequently, compared to previous methodologies, the LPV modeling and event-triggered control synthesis for boost converters deliver several advantages, including faster dynamics and lower control utilization.

This chapter has presented an event-triggered control strategy for the LPV framework of a boost converter, incorporating the establishment of an appropriate triggering condition. The design of the controller, contingent on the duty ratio, contributes to an improved voltage regulation performance. Stability was demonstrated for the closed-loop system comprising the boost converter and the parameter-dependent controller. Simulation and experimental results are provided for two scenarios: (i) variations in input voltage and (ii) changes in load currents. In both scenarios, the controller exhibited favorable performance, significantly reducing the need for control updates and minimizing the utilization of computational and communication resources. A lower bound on the inter-event time is also introduced to eliminate Zeno behavior.